Pressure Loss through Rock Fracture Intersections

Danny Hermawan, Tom Brooks, and Mathieu Sellier

University of Canterbury, Private Bag 4800, Christchurch, New Zealand

dhe48@uclive.ac.nz

Keywords: *fractures, fluid flow models, geothermal reservoirs, pressure loss*

ABSTRACT

Over time, the extraction and reinjection of geothermal fluid to generate electricity results in a decrease in the overall pressure of a geothermal reservoir. This results in the precipitation of minerals that cause blockages in the power station equipment and the rock fractures in the reservoir; as well as a lower flow rate available for electricity generation. A better understanding of fluid flow in a fracture network is required to better predict the performance of the reservoir over time. This paper aims to determine a relationship for the pressure loss of flow through the intersection of two rock fractures connected end-to-end. The model uses an electrical circuit analogy, where the pressure loss of the intersection is equivalent to an additional electrical resistance in a fractured network. Computational Fluid Dynamics (CFD) simulations were carried out for various aspect ratios, Reynolds numbers and the angle of orientation of the two fractures. Using data fitting methods, a general expression was found linking the pressure loss, Reynolds number, and angle of orientation, given a specific aspect ratio. The model was able to predict three fracture in series within 14% accuracy.

1. INTRODUCTION

Geothermal systems play an important role in supplying renewable energy in a world that is gradually shifting away from using unsustainable fossil fuels. Approximately 13% of New Zealand's electricity is generated from geothermal sources (NZGA, 2016), with this set to increase as investment in geothermal energy grows to meet the 90% renewable electricity generation by 2025 (MED, 2011). Most geothermal energy comes from the superheated hydrothermal fluid within the Earth's crust. As the fluid permeates into fractured rock, it serves as a conduit for fluid flow and a geothermal reservoir is formed.

An Enhanced Geothermal System (EGS) is defined as an engineered geothermal reservoir that is used to extract heat from the subsurface by drilling a production well into the reservoir. The extracted superheated fluid undergoes a thermal cycle, and get reinjected back into the reservoir through an injection well. This creates a closed loop system that maintains the pressure gradient through the reservoir (MIT, 2016), which becomes the main driver for fluid flow through the fracture network. Over time, the pressure decreases in the reservoir as fluid is extracted much faster than the time it takes for the reinjected fluid to make its way through the fracture network and reheat (Grant & Bixley, 2011). Thus, an understanding of the overall performance of a reservoir is required in design of a geothermal power plant (Ogino & Yamamura, 1996)

Fracture properties can change during the operation of reservoir due to fluid pressure changes, thermal cooling, and precipitation of minerals (NRC, 1996). Geothermal fluids contain dissolved minerals, such as silica, that do not precipitate out at the high temperatures and pressures in the reservoir. Due to the decrease in pressure as the fluid makes its way to the surface, these minerals start to precipitate, causing blockages in the power plant equipment. Precipitation also occurs in the fractures themselves (due to the decrease in the overall pressure of the reservoir), restricting the flow in the rock fractures (Grant & Bixley, 2011). This results in a decrease in the fluid flow rates over the useable lifespan of the reservoir. Therefore, it is of interest to model the fluid flow through a geothermal fracture network to gain a better understanding of the flow properties in a fracture network.

Understanding the fracture network through modeling has been rigorously studied (Witherspoon, 1980; Zhao et al., 2011; Frampton and Cvetkovic, 2007; Sarkar, 2002; Kristinof et al., 2010; Kissling et al., 2015; Doe et al., 2014; Liu et al. 2016). Common methods of fracture network modeling, such as discreet fracture network (DFN), continuum model, Voronoi diagram, Hele-Shaw approximations, and percolation theory (NRC, 1996), are often used to simplified the quantification and analysis of the transport phenomenon. The flow characteristics, which often simplified to the 'cubic law' (Witherspoon, 1980) were investigated with regards to the fluid properties and fracture geometries.

This research aims to determine a relationship for the pressure loss of the flow through the intersection of two fractures connected end to end. This will allow for a simplification in fracture network models as the pressure loss due to fracture intersections can be easily calculated and hence accounted for in any results. Previous studies on pressure perturbation caused by fractures have been done in a 2D setting. However, the pressure loss due to an intersection of fractures has not been studied. The pressure loss through each individual fracture due to frictional effects, as well as that for the intersection, can be thought of as being similar to that of an electrical resistor network. A fracture network can consist of fractures in series and parallel, while the intersection of two fractures is in series with the fractures themselves, as shown in Figure 1. This analogy can be used to create a network of fractures and fracture intersections, of which the total pressure loss can be calculated by adding up the individual pressure loss for each fracture and fracture intersection.

2. MODELLING METHODOLOGY

This paper focuses on the intersection of two rectangular fractures connected end to end and orientated at some angle α to each other, as shown in Figure 1.

In Figure 1, a_1, a_2, w_1, w_2, L_1 and L_2 are the apertures, widths and lengths of the upstream and downstream fractures respectively. The aspect ratio of the fracture geometry is defined as:

$$AR = \frac{w}{a} \quad (1)$$

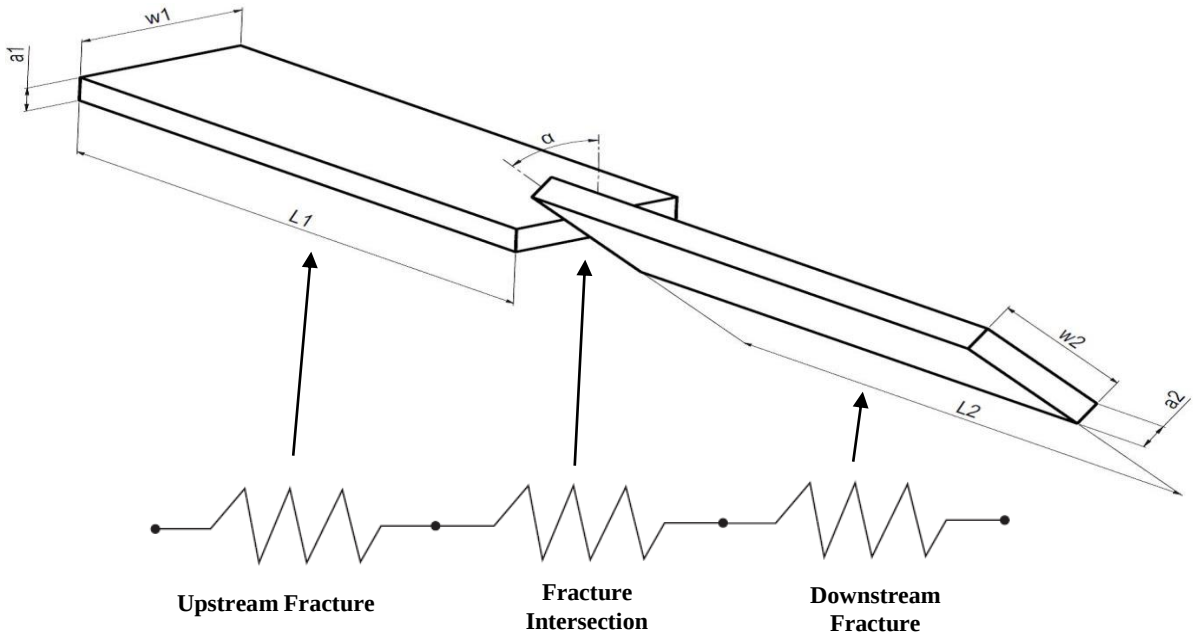

Figure 1: Fracture Geometry used in Models along with Electrical Resistor Network Analogy.

For this study, the aperture and width of both the upstream and downstream fractures are assumed to be equal, so:

$$a_1 = a_2 = a$$

$$w_1 = w_2 = w$$

$$AR_1 = AR_2 = AR$$

The values of L_1 and L_2 were different for each model simulated and determined by the entrance length required for the flow to become fully developed in each fracture.

The flow through two fractures connected end to end can be represented by flow in rectangular ducts and modelled by the Navier-Stokes (NS) equations. As the scale of fracture networks can be in the order of kilometres, it would be more suitable to use smaller scale models to keep the size of the computational model as small as possible. Therefore, the non-dimensional NS equations are required so that the flow can be modelled for any scale of fracture geometries and flow properties while keeping the computational time down. A steady, incompressible flow can be modelled by the NS and continuity equations:

$$\rho\mathbf{V}\cdot\nabla\mathbf{V} = -\nabla p + \mu\nabla^2\mathbf{V} + \rho\mathbf{g}$$

$$\nabla\cdot(\rho\mathbf{V}) = 0$$

Where $\mathbf{V}$ is the flow velocity vector, p is the pressure, μ is the dynamic viscosity, ρ is the density and $\mathbf{g}$ is the gravity vector. The steady, incompressible dimensionless NS equations are represented in general form by:

$$\nabla\mathbf{V}^* = -\nabla p^* + \frac{1}{Re}\nabla^2\mathbf{V}^* + \frac{1}{Fr^2}\mathbf{g}^* \quad (2)$$

Where * denotes a dimensionless quantity, Re is the Reynolds number and Fr is the Froude number. The dimensionless quantities are defined as:

$$p^* = \frac{p}{\rho {V_0}^2}$$

$$\mathbf{V}^* = \frac{\mathbf{V}}{V_0}$$

$$\mathbf{g}^* = \frac{\mathbf{g}}{g_0}$$

$$Re = \frac{\rho d_h}{\mu}$$

$$Fr = \frac{V_0}{\sqrt{g_0 d_h}}$$

The subscript zero denotes the characteristic dimensional scale, and, d_h is the hydraulic diameter (characteristic length scale).

Initially, a physical domain was created by choosing values for *a* and *w* to give a certain aspect ratio. To convert the physical domain to the dimensionless domain, *a* and *w* needed to be divided by the characteristic length. For ducted flow, the characteristic length is the hydraulic diameter, d_h; which was calculated in the physical domain and used to find the values of *a* and *w* in the dimensionless domain (a_D and w_D respectively).

To carry out flow simulations in the dimensionless domain, a computational domain was created because dimensionless numbers cannot be used in Computational Fluid Dynamics (CFD) software where dimensional values are required. For this model, the computational domain consisted of matching the coefficients of the dimensionless NS equations to the coefficients of the dimensional NS equations, allowing for use of dimensionless values in the CFD software. The dimensionless flow inlet velocity (U) and density (ρ) both

had values of unity, while the μ had a value of the inverse of Re as per Equation 2. Therefore, in the computational domain, they were held constant at 1 ms^{-1} and 1 kgm^{-3} respectively, while μ varies as Re was changed. The lengths L_1 and L_2 were set in the computational domain, rather than the physical domain, as the length for the flow to become fully developed depends on the quantities used in the computational domain.

Using ANSYS CFX simulation software, the geometry in Figure 1 was created for the required values of a_D, w_D, L_1, and L_2 to give a particular AR. Overall, the geometries in the computational domain were large in scale, with fracture lengths ranging from 12 to 70 m, and widths ranging from three to 13 m. A structured hexahedral mesh was used to discretise the geometry. The element size on the two intersecting faces was set to 50 mm, while for fractures one and two, the element size was set to 250 mm and 100 mm respectively. The element size in the upstream fracture was larger than that of the downstream fracture because vortices exist due to the sudden expansion; therefore, a finer mesh was required to fully capture the flow. The mesh size is relatively small to the overall geometry to increase the accuracy of the pressure field. The number of elements used depended on the aspect ratio being modelled, and ranged from $8x10^5$ to $25x10^5$ for those modelled in this study. A mesh convergence study was conducted to see the sensitivity of the solution to the number of elements in the simulation. Figure 2 shows an asymptotic relationship between the pressure and the elements number, which translates to the accuracy of the solution as the simulation result converges to a limit. The number of elements used in the subsequent simulations are in the range of $8x10^5$ elements.

The boundary conditions for the model consisted of an inlet velocity of one, outlet reference pressure of zero, and smooth, no-slip walls. Figure 3 shows the locations of the boundary conditions on the geometry. As the Re was an independent variable in the model, an input parameter was created so that an expression for calculating the μ could be set up in ANSYS CFX-Pre. A custom fluid was created for the dimensionless fluid properties could be included in the computational domain (ρ=1 kgm^{-3}, μ as calculated from Re).

An assumption of this model was that the flow was laminar. As the fracture intersection has the smallest area that the fluid can flow through, the velocity is greatest due to mass conservation. This means that the Re at the intersection cannot exceed 2060 (Hanks & Ruo, 1966) if the flow is to remain laminar. Using the maximum AR of 25 in this study, the Re at the inlet was calculated to be 150 for a Re of 2000 at the intersection. Therefore, the maximum value of Re is 150 in this study.

ANSYS CFX finite volume code was used to solve the governing flow equations. Residuals of 10^{-4} were used to determine convergence, which occurred after approximately 45 iterations. For some simulations, the residuals started to increase before the convergence criteria was met, thus increasing the solve time. To keep the solve time to a minimum, an upper limit of 50 iterations was set, with the difference between this result and the result calculated when convergence criteria was met being less than 0.2 Pa.

The pressure loss due to the fracture intersection was calculated by first obtaining the change in pressure at the inlet compared to the outlet. During post-processing of the results, an expression that calculated the average pressure at the inlet and subtracted the average pressure at the outlet was used to calculate the pressure loss across the whole model. The head loss, h_f, and hence pressure loss, ΔP_f, in a non-circular duct was calculated by:

$$h_f = f\frac{LV^2}{2D_h g}$$

$$\Delta P_f = \rho g h_f$$

Where $f = \frac{64}{Re}$ for laminar flow, L is the length of the fracture, V is the inlet velocity and g is the acceleration due to gravity (White, 2011). ΔP_f due to wall friction in the upstream and downstream fractures was subtracted from the pressure loss results. Therefore, the remaining pressure loss is a result of the fracture intersection.

The pressure loss, ΔP, through the intersection of two horizontal fractures connected end-to-end is a function of the following parameters:

$$\Delta P = f(a, w, L_1, L_2, \rho, U, \alpha)$$

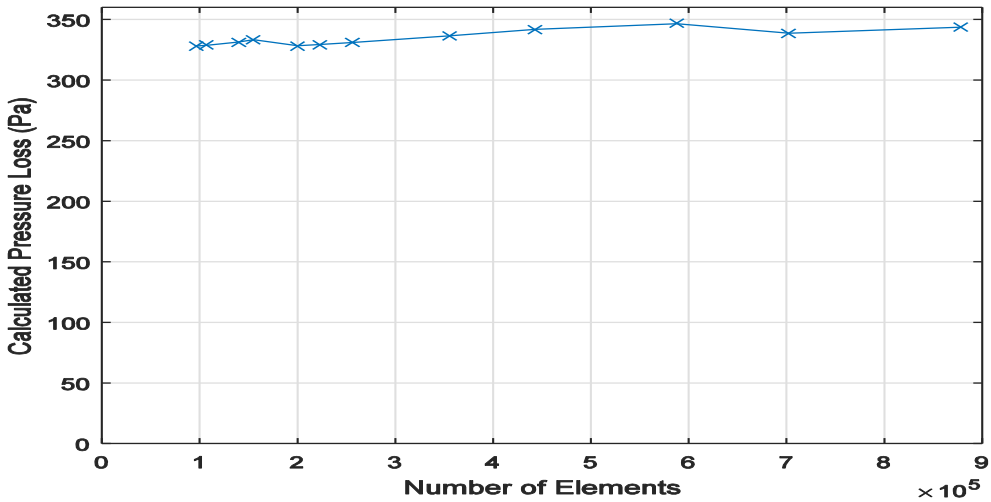

Figure 2: Mesh Convergence for Geometry with AR=25 and Re=150.

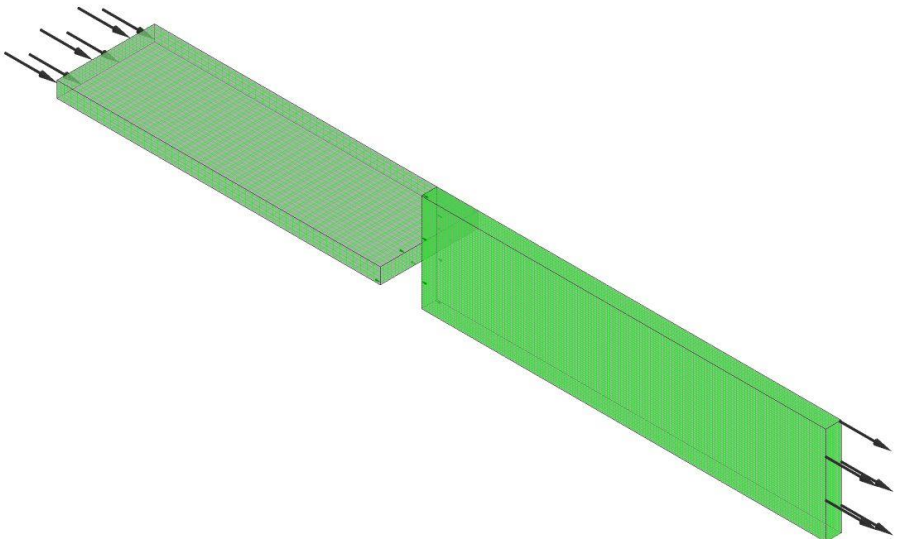

Figure 3: Location of Model Boundary Conditions.

As the pressure loss due to the fracture intersections is of interest only, the pressure loss due to the length of each fracture is subtracted from the results of the model. Therefore, pressure loss is now only a function of five variables:

$$\Delta P = f(a, w, \rho, U, \alpha)$$

Using ρ, U and a as repeating variables, the Buckingham Pi method can be used to create four dimensionless Π groups:

$$\Pi_1 = \frac{\Delta P}{\rho U^2}$$

$$\Pi_2 = \frac{\mu}{\rho U a}$$

$$\Pi_3 = \alpha$$

$$\Pi_4 = \frac{w}{a}$$

As the values of density and velocity are one, an expression for the pressure loss in terms of the other Π groups is:

$$\Delta P = f\left(\frac{\mu}{a}, \alpha, \frac{w}{a}\right)$$

Given that the μ was previously defined as the inverse of the Re, and the AR defined as the width divided by aperture, then the pressure loss resulting from the fracture intersection is a function of the Re, α and the AR. It was assumed here that the fractures are horizontal, hence the effect of gravity was negligible. However, the effect of gravity will be investigated later. Using the correlation described in the paper, the pressure loss was estimated to be 44.

For this paper, seven different AR ranging from 6.25 to 25 were defined, resulting in seven different fracture geometries. For each AR, a parametric study in ANSYS Workbench was carried out for 10 different Re ranging from 10 to 150. For each Re, the α was increased from 0 to 88° in increments of 2°. This resulted in 3150 individual simulations being carried out.

Once the simulations were completed for one AR, the four Π groups were created. Using the MATLAB curve fitting toolbox, a surface was fitted to the data. This resulted in a polynomial equation for a surface for each different AR.

3. RESULTS AND DISCUSSION

For each geometry, a visual check of the flow was carried out before commencing the parametric study to ensure that the model was working correctly. This was achieved in post-processing by plotting the velocity streamlines through the fracture geometry. The flow through the fracture intersection is essentially a sudden contraction followed by a sudden expansion. At low Re, two regions of separation occur above and below the intersection in the downstream fracture as the flow suddenly expands (Durst, Pereira, & Tropea, 1993). Therefore, by plotting the velocity streamlines, one can check for the two regions of separation and vortices in thw downstream fracture. Figure 4 shows the flow through the fracture geometry for an aspect ratio of 25 and Re of 150. As can be seen in Figure 4, there are two vortices in the downstream fracture that result from the region of separation caused by the flow's sudden expansion into the fracture.

After creating the four Π groups from the resulting data, Π_2 and Π_3 were each plotted against Pi_1 for each aspect ratio to determine any individual relationships. As can be seen in Figure 5, there is a linear relationship between Π_1 and Π_2, while in Figure 6, there is a trigonometric relationship between Π_1 and Π_3, which is expected due to the presence of the α in Π_3. The trigonometric relationship in Figure 6 represents that of a cosine function. Taking the cosine of Π_3 and plotting against Π_1 shows a quadratic relationship, as shown in Figure 7. As there is a quadratic relationship, creating a surface between the three Π groups is much easier as a polynomial fit can be used.

Using the values of Π_2, $\cos(\Pi_3)$ and Π_1 as the x, y and z co-ordinates respectively in the MATLAB curve fitting toolbox, a polynomial fit was applied to create an equation for the surface that fits the data for a specific AR. The polynomial fit was degree one for Π_2 and degree two for $\cos(\Pi_3)$ due to the linear and quadratic relationships with Π_1 respectively.

Figure 4: Flow Velocity Streamlines for Geometry with AR=25, Re=150.

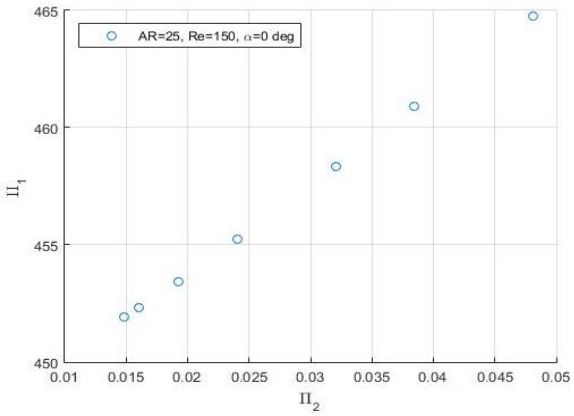

Figure 5: Linear Relationship between Π_1 and Π_2 Shown for the Case of AR=25, Re=150 and α=0°.

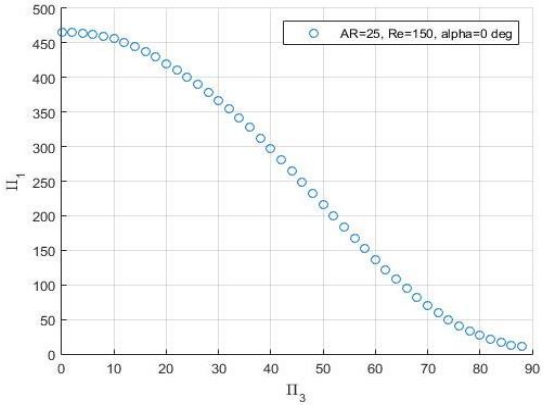

Figure 6: Trigonometric Relationship between Π_1 and Π_3 Shown for the Case of AR=25, Re=150.

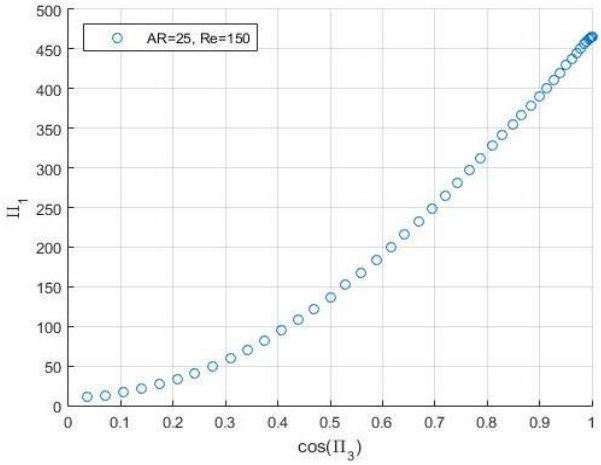

Figure 7: Quadratic Relationship Between Π_1 and cos(Π_3) Shown for the Case of AR=25, Re=150.

From the curve fitting process, the coefficients can be determined for the general equation:

$$\Pi_1 = C_1 + C_2\Pi_2 + C_3\cos(\Pi_3) + C_4\Pi_2\cos(\Pi_3) + C_5(\cos(\Pi_3))^2 \quad (3)$$

Where C_1, C_2, C_3, C_4 and C_5 are the coefficients given as an output by MATLAB.

Figure 8 shows the data fitted to a polynomial surface, with an R^2 value of 0.9995. This surface fitting process was conducted for all seven AR, with the resulting coefficients shown in Table 1.

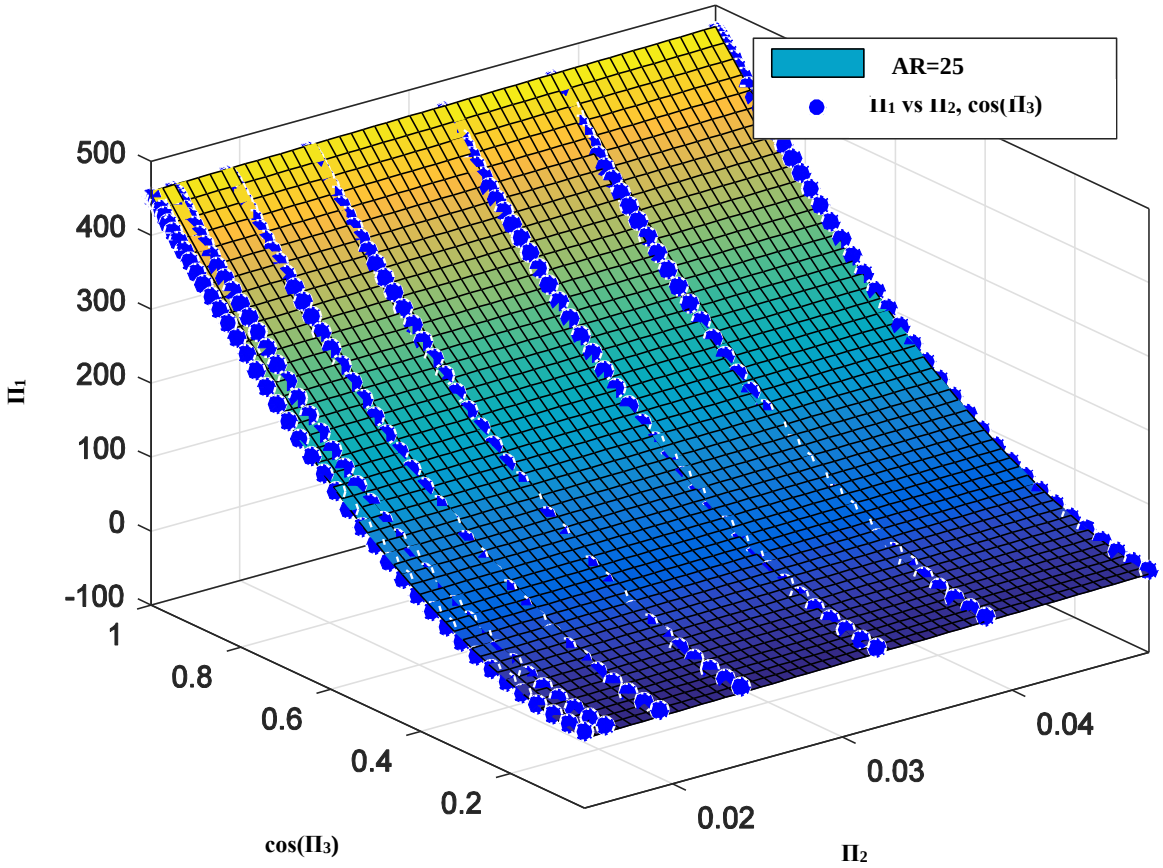

Figure 8: Polynomial Surface fitted to Data for AR=25.

Table 1: Coefficients for Polynomial Equation for each Aspect Ratio

Aspect Ratio	C_1	C_2	C_3	C_4	C_5	R^2
6.25	0.463	68.4	-8.03	70.2	33.9	0.998
8.33	-0.979	148.3	-0.97	65.01	48.2	0.995
10	-2.18	136.3	5.47	117.4	62.9	0.999
12.5	-2.12	234.3	0.725	47.08	113.3	0.9998
15	-6.94	242.8	31.5	150.7	131.1	0.998
20	-12.5	377.8	63.1	144.7	231.3	0.9985
25	-13.8	343.8	74.6	15.5	393.1	0.9995

Overall, the model can be used for Re and AR up to 150 and 25 respectively. Values higher than these means that the model is extrapolating beyond its upper bounds and further validation would be required. For Re greater than 150, the flow can become turbulent at the fracture intersection. When setting up the model, the assumption of laminar flow was made, so once the flow becomes turbulent, the model becomes invalid. Therefore, if the upper limits of the AR and Re are not exceeded, then the flow is laminar through the fracture intersection and the model remains valid.

Further investigation into the relationship of the aspect ratio and the coefficients of the general equation (Eq. 3) does not yield conclusive relationship. Three coefficients does show a good relationship with the AR, however two coefficients show significant variations when plotted with AR. There seems to be a discontinuity in the relationship. When plotting the five coefficients against small value of AR (AR < 11), good fitting relationships are observed in all of them. Similar trend was observed when plotting the five coefficients with

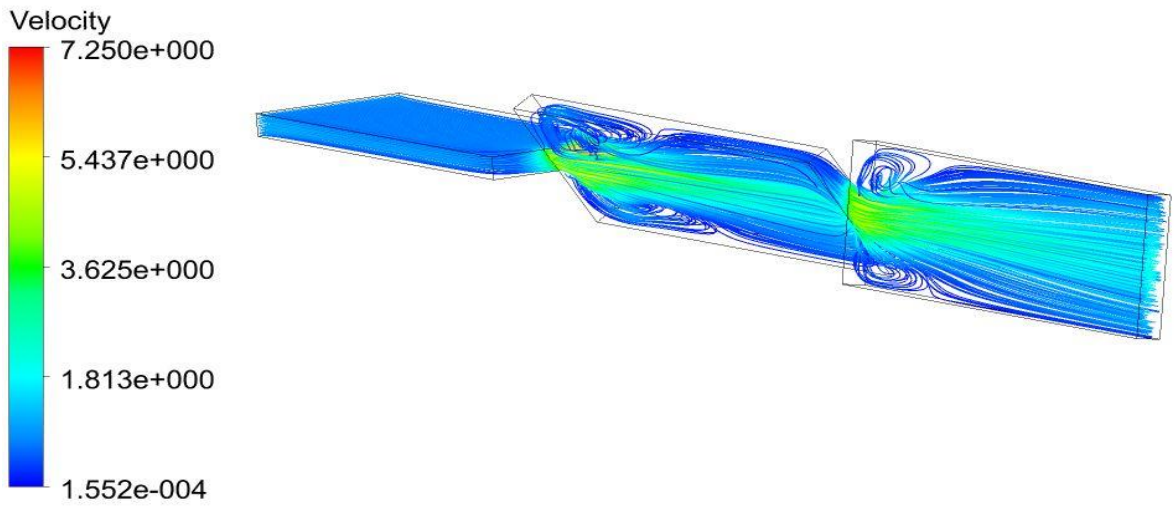

Figure 9: Three Fractures in Series.

high value of AR (AR > 12.5), however the trend does not seem to be continuous when compared to the low AR values. This may indicate that the flow enters a different regime at the intersection due to the sudden contraction.

Three fractures in series were simulated to test the validity of the model in predicting the pressure loss in the two intersections (Figure 9). The angle of orientations were 30° and 20° with respect to the previous fracture. The AR and Re were set to 6.25 and 150 respectively. The simulation results in a pressure loss of 36.0 Pa for the two intersections. The correlation described in this paper estimates a pressure loss of 41.0 Pa, which has an error of 14%.

In finding the source of error, the precision of the correlation was investigated. The fractures with AR = 6.25 all showed an error of less than 5% with some exceptions of those with angle of intersection greater than 76°. Therefore, it was possible that the three fractures in series have a higher error because the flow in the second fracture was underdeveloped as it went to another intersection. Since the correlation was built with a developed flow, the predicted pressure loss would contain error. Further investigation is required to validate the model with more fractures in series.

In determining the effect of gravity, the geometric model was modified to include a parameter for the angle, β, of the two fractures from the horizontal. The same process was carried out as with the original simulations, except gravity was now defined. By Bernoulli's Equation, gravity will have an overall effect on the flow as a whole as there will be some head loss as the flow changes height (White, 2011). As only the pressure loss due to the fracture intersection is of interest, then the pressure loss due to the head loss will also be subtracted from the CFD simulation result; similar to that for the wall friction pressure loss. Therefore, it was expected that there would be little difference in the intersection pressure loss as β increased. As can be seen in Figure 12, this was the case.

Further work is required to determine how well the model is able to predict the pressure losses for a larger number of fractures in series, as well as fracture networks consisting of fractures both in series and parallel. Experimental tests could also be conducted to validate both CFD model and the mathematical model proposed. This could be carried out by

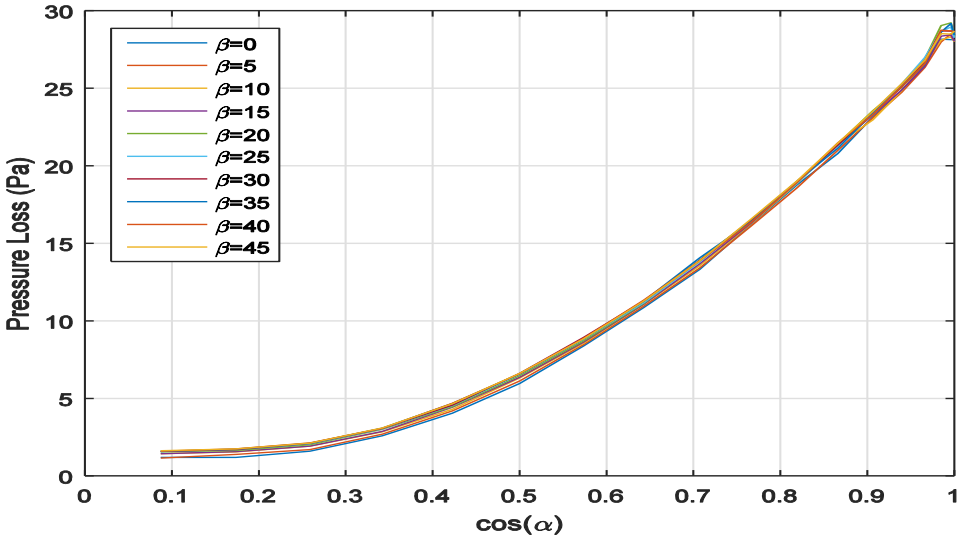

Figure 10: Pressure Loss when Considering Gravity for AR=6.25, Re=150 and a=0.

creating a test right that uses parallel plates to represent the fractures and measuring the pressure difference of the flow from the inlet to the outlet.

CONCLUSION

In calculating the pressure loss for flow passing through a fracture intersection, a series of CFD simulations were carried out for varying AR, Re and α. Using data fitting methods, a polynomial relationship was found for the pressure loss in terms of the Re and α for a specific AR. When using the model to determine the fracture intersection, pressure losses from three fractures in series, there was a 14% difference in the pressure loss when compared to directly modelling the fractures in a CFD analysis. Further work is required to determine how the model performs for a larger number of fractures, as well as for networks of fractures both in series and parallel.

REFERENCES

Berkowitz, B. (2002). Characterizing flow and transport in fractured geological media: A review. *Advances in Water Resources, 25*, 861-884.

Doe, T., McLaren, R., & Dershowitz, W. (2014). Discrete Fracture Network Simulations of Enhanced Geothermal Systems. *PROCEEDINGS, 39th Workshop on Geothermal Reservoir Engineering*. Stanford: Stanford University.

Durst, F., Pereira, J., & Tropea, C. (1993). The Plane Symmetric Sudden Expansion Flow at Low Reynolds Numbers. *Journal of Fluid Mechanics*, 567-581.

Frampton, A., & Cvetkovic, V. (2007). Upscaling Particle Transport in Discrete Fracture Networks: 1. Nonreactive Tracers. *Water Resources Research*.

Graham, I. J. (2008). *A Continent on the Move: New Zealand Geoscience into the 21st Century*. Wellington: Geological Society of New Zealand.

Grant, M., & Bixley, P. (2011). *Geothermal Reservoir Engineering*. Elsevier Inc.

Hanks, R. W., & Ruo, H.-C. (1966). Laminar-Turbulent Transition in Ducts of Rectangular Cross Section. *Industrial & Engineering Chemistry Fundamentals*, 558-560.

Kissling, W., Ellis, S., McNamara, D., & Massiot, C. (2015). Modelling Fluid Flow Through Fractured Rock: Examples Using TVZ Geothermal Reservoirs. *Proceedings 37th New Zealand Geothermal Workshop*. Taupo: NZGW.

Kristinof, R., Ranjith, P., & Choi, S. (2010). Finite element simulation of fluid flow in fractured rock media. *Environ Earth Sci, 10*, 765-773. doi:DOI 10.1007/s12665-009-0214-2

Liu, R., Jiang, Y., & Li, B. (2016). Effects of Intersection and Dead-end of Fractures on Nonlinear Flow and Particle Transport in Rock Fracture Networks. *Geosciences Journal*, 415-426.

Ministry of Economic Development. (2011, August). *Energy*. Retrieved from Ministry of Business, Innovation & Employment: http://www.mbie.govt.nz/info-services/sectors-industries/energy/documents-image-library/nz-energy-strategy-lr.pdf

MIT. (2016). *The Future of Geothermal Energy: Impact of Enhanced Geothermal Systems on the United States in the 21st Century*. Masssachusetts Institute of Technology.

National Research Council (NRC). (1996). *Rock Fractures and Fluid Flow*. Washington: National Academy press.

New Zealand Geothermal Association (NZGA). (2016). *Geothermal Energy & Electricity Generation*. Retrieved from NZ Geothermal Association: http://nzgeothermal.org.nz/elec_geo/

Ogino, F., & Yamamura, M. (1998). Pressure Drop of Water Flow Between Injection and Production Wells Intersected By A Circular Fracture. *Geothermics, 27*(1), 25-41.

Sarkar, S., Nafi Toksoz, M., & Burns, D. R. (2002). *Fluid Flow Modeling in Fractures*. Massachusetts Institute of Technology, Earth Resources Laboratory, Cambridge.

White, F. (2011). *Fluid Mechanics*. New York: McGraw Hill.

Wilson, C., & Witherspoon, P. (1976). Flow Interference Effects at Fracture Intersections. *Water Resources Research*.

Witherspoon, P., Wang, J., Iwai, K., & Gale, J. (1980). Validity of cubic law for fluid flow in a deformable rock fracture. *Water Resour Res, 16*, 1016-1024.

Zhao, Z., Jing, L., Neretnieks, I., & Moreno, L. (2011). Numerical Modelling of Stress Effects on Solute Transport in Fractured Rocks. *Computers and Geotechnics*, 113-126.